

MoRPI-PINN: A Physics-Informed Framework for Mobile Robot Pure Inertial Navigation

Arup Kumar Sahoo and Itzik Klein

Abstract—A fundamental requirement for full autonomy in mobile robots is accurate navigation even in situations where satellite navigation or cameras are unavailable. In such practical situations, relying only on inertial sensors will result in navigation solution drift due to the sensors’ inherent noise and error terms. One of the emerging solutions to mitigate drift is to maneuver the robot in a snake-like slithering motion to increase the inertial signal to noise ratio allowing the regression of the mobile robot position. In this work, we propose MoRPI-PINN as a physics-informed neural network framework for accurate inertial-based mobile robot navigation. By embedding physical laws and constraints into the training process, MoRPI-PINN is capable of providing an accurate and robust navigation solution. Using real-world experiments, we show accuracy improvements of over 85% compared to other approaches. MoRPI-PINN is a lightweight approach that can be implemented even on edge devices and used in any typical mobile robot application.

Index Terms—Scientific Machine Learning; Physics-informed Neural Networks; Inertial Navigation System; Mobile Robot; Accelerometer; Gyroscope; Yaw Angle; Dead Reckoning.

TABLE
LIST OF ABBREVIATIONS

Abbreviation	Definition
Navigation	
INS	Inertial Navigation System
IMU	Inertial Measurement Unit
GNSS	Global Navigation Satellite System
RTK	Real-Time Kinematic
NED	North-East-Down (Coordinate Frame)
ECEF	Earth-Centered Earth-Fixed
Neural Networks	
PINN	Physics-informed Neural Network
AD	Automatic Differentiation
GT	Ground Truth
Error Metrics	
ATE	Absolute Trajectory Error
MATE	Mean Absolute Trajectory Error
MSE	Mean Squared Error
RMSE	Root Mean Squared Error
NRMSE	Normalized Root Mean Squared Error

I. INTRODUCTION

A. K. S. is supported in part by the Maurice Hatter Foundation. (Corresponding author: Arup Kumar Sahoo)

The authors are with the Autonomous Navigation and Sensor Fusion Lab (ANSFL), the Hatter Department of Marine Technologies, Charney School of Marine Sciences, University of Haifa, Haifa 3498838, Israel. (e-mail: asahoo@campus.haifa.ac.il, itzik@univ.haifa.ac.il)

THE study of mobile robots is crucial for modern industries and services, as they are deployed across various fields. It includes logistics, transportation, agriculture, health-care, military operations, and data collection in hazardous environments [1], [2], [3], and [4]. In recent years, the market demand of mobile robots have been significantly increased, because of increase in application areas, advances in robot technology along with the cost reductions in electronic sensors and devices. As a result, around the globe, various companies are developing mobile robots to meet these demands and explore new markets.

Navigation plays a fundamental role in mobile robot design, enabling precise determination of position and orientation across diverse and often challenging environments. While operating outdoors, the navigation task depends on a variety of sensors, including cameras [5], LiDAR [6], Sonar [7], global navigation satellite systems (GNSS) [8], inertial navigation system (INS) [9], and odometers [10]. In indoors or tunnels the GNSS signals are unavailable while vision methods suffer from poor lighting conditions or featureless environments. In such real-world scenarios, the navigation solution depends only on the inertial sensor readings in a process known as pure inertial navigation [11], [12].

There, the navigation solution drifts due to errors and noise in the inertial measurement. To cope with the inertial drift Shurin and Klein [13] proposed the quadrotor dead-reckoning approach. Inspired by the natural movement of pedestrians [14], [15], they enforced periodic motion on quadrotors and designed a model-based approach for positioning. Later, similar model-based approaches were applied on mobile robots [16]. With the emergence of deep-learning approaches in the navigation field [17], [18], neural network solutions were designed for quadrotors [19] and mobile robots [20].

Recent advances in scientific machine learning, offers promising solutions to such challenges and uncovers novel scientific phenomena, particularly through physics-informed neural networks (PINNs). Unlike conventional deep neural networks (DNNs), PINNs embed physical laws typically expressed as differential equations (DEs) directly into the objective function of neural network as a residual loss [21]. This integration ensures that model outputs adhere to governing physical principles, enhancing accuracy and interpretability while reducing reliance on extensive labeled data. PINNs leverage parallel computing and automatic differentiation, in order to address the computational inefficiencies of repeatedly solving DEs. In past few years, PINNs have demonstrated remarkable success across scientific and engineering domains, including anomaly detection [22], [23], fluid mechanics [24], solid mechanics

[25], remote sensing [26], robot manipulation [27], [28], and beyond. These advances highlight PINNs as a powerful tool for modeling complex dynamical systems, particularly where traditional methods struggle due to noisy data. In the domain of navigation and control, Xu et al. [29] developed a PINN-based model for the prediction in sway and surge velocities, as well as rotational speed in the unmanned surface vehicles. In a recent work, Park and Lee [28] employed PINN algorithm with error tracking control to estimate the speed of the leader robot.

Building on the PINN advancements, this paper introduces MoRPI-PINN, a mobile robot pure inertial framework for accurate navigation. It is hypothesized that PINNs can effectively guide the model using partial physical knowledge in the form of ordinary or partial differential equations and limited data. PINNs offer a unified framework for such scenarios by embedding known physical laws (e.g., 2D-INS equations here) directly into neural network training. This is achieved through automatic differentiation enforcing the governing differential equations as soft constraints in the loss function. In inertial navigation, MoRPI-PINN model learn the system's trajectory by balancing physical consistency and data fidelity. This makes them particularly suitable for navigation tasks with limited and/or noisy sensor data. To further increase the influence of our MoRPI-PINN framework, we constrain the robot to move in a snake-like slithering motion, as this motion has already proven to yield an increased inertial signal to noise ratio allowing regression of the mobile robot's position, even in rough terrain.

The contributions of this paper are:

- Development of the MoRPI-PINN framework to cope with real-world scenarios of pure inertial navigation for mobile robots operating in various scenarios.
- Integration of the governing physics of 2D-INS equations of motion with sparse sensor data, relying only on a single trajectory, during the training process of the network.

We demonstrate that by embedding the physical laws and constraints of 2D-INS equations of motion into the training process, MoRPI-PINN provides an accurate and robust navigation solution for a mobile robot. Using real-world experiments on a mobile robot equipped with IMU and RTK-GNSS, we present an 85% improvement over other model-based and data-driven methods.

The rest of the paper can be outlined as follows: Section II presents the INS equation and various model based solutions. Section III gives our proposed approach, detailing the formulation of PINNs algorithm and model architecture. Section IV describes our experimental setup and presents comprehensive results, with analyses of the data. Finally, the conclusions are drawn in Section V.

II. MODEL-BASED APPROACHES

This section provides a brief overview of 2D-INS model-based solutions and MoRPI-PINN prediction, that has been later used as baselines for comparison with our proposed MoRPI-PINN approach.

A. Inertial Navigation System

An inertial navigation system provides a comprehensive navigation solution, encompassing position, velocity, and orientation. Moreover, the fundamental INS equations of motion are often formulated within a navigation frame (n-frame) using north-east-down (NED) coordinates. But for practical mobile robot navigation, a more convenient local frame (l-frame) is typically employed. This l-frame is defined at the starting location of robot, with its axes aligned to the north, east, and down directions. The INS equations of motion are given by [16]:

$$\dot{\mathbf{p}}^n = \mathbf{v}^n, \quad (1)$$

$$\dot{\mathbf{v}}^n = \mathbf{C}_b^n \mathbf{f}_{ib}^b + \mathbf{g}^n, \quad (2)$$

$$\dot{\mathbf{C}}_b^n = \mathbf{C}_b^n \mathbf{\Omega}_{ib}^b. \quad (3)$$

Where in (1)–(3), \mathbf{p}^n denotes the position vector in the l-frame, \mathbf{v}^n represents the velocity vector in the same frame, and \mathbf{g}^n is the gravity vector, which is assumed to be constant throughout the trajectory. The matrix \mathbf{C}_b^n is an orthonormal rotation matrix that transforms vectors from the body frame (b-frame) to the n-frame. The specific force \mathbf{f}_{ib}^b is measured by the accelerometer in the b-frame, while $\mathbf{\Omega}_{ib}^b$ is a skew-symmetric matrix representing the angular rate measured by the gyroscope.

The accelerometer measures the specific force in the b-frame, represented by the vector:

$$\mathbf{f}_{ib}^b = [f_x \quad f_y \quad f_z]^T, \quad (4)$$

where f_x, f_y, f_z are the accelerometer readings along the b-frame axes.

Similarly, the gyroscope measures the angular velocity in the b-frame as:

$$\omega_{ib}^b = [\omega_x \quad \omega_y \quad \omega_z]^T. \quad (5)$$

Here, $\omega_x, \omega_y, \omega_z$ are the components of the angular rate vector. The subscript ib indicates measurement relative to the l-frame, while the superscript b denotes resolution in the b-frame. The skew-symmetric angular rate matrix $\mathbf{\Omega}_{ib}^b$ is defined as:

$$\mathbf{\Omega}_{ib}^b = \begin{bmatrix} 0 & -\omega_z & \omega_y \\ \omega_z & 0 & -\omega_x \\ -\omega_y & \omega_x & 0 \end{bmatrix}, \quad (6)$$

where $\omega_x, \omega_y, \omega_z$ are the components of the angular velocity vector ω_{ib}^b .

B. Wheeled Robot Motion Model

For wheeled robot motion, it is commonly assumed that the roll and pitch angles are negligible, with movement primarily occurring in the x - y plane. Under this assumption, the body-to-navigation frame transformation depends solely on the yaw angle ψ , and is given by [30]:

$$\mathbf{C}_b^n = \begin{bmatrix} \cos \psi & -\sin \psi & 0 \\ \sin \psi & \cos \psi & 0 \\ 0 & 0 & 1 \end{bmatrix}. \quad (7)$$

Substituting (7) into (2) shows that f_z has no influence on position or velocity in the horizontal plane. Thus, it can be excluded from inertial calculations. Additionally, since only the yaw angle is relevant, the gyroscope components ω_x and ω_y

are neglected, and only ω_z is retained. Furthermore, due to the use of low-cost inertial sensors and the relatively short time intervals involved, both the Earth's rotation rate and transport rate are neglected in (2)–(3).

C. MoRPINet

MoRPINet is a state-of-the-art data driven model specifically designed for pure inertial positioning approach of mobile robot. It leverages the serpentine dynamic motion of mobile robots and follows a three-phase process for dead-reckoning position updates. It can be listed as:

- **Distance Estimation:** A neural network architecture viz. D-Net is introduced for distance regression. It combines one-dimensional convolutional layers (1D-CNN) with a fully connected output layer to estimate distance using only inertial sensor data.
- **Heading Estimation:** The widely used Madgwick filter is employed to determine heading based on inertial measurements. Moreover, the Madgwick filter depends on two parts: (1) orientation from angular rate, and (2) orientation from vector observations.
- **Position Update:** Finally, the position is updated through dead reckoning, utilizing the distance and heading estimates obtained from the previous steps. The update has been performed using the following equations:

$$x_{k+1} = x_k + s_{\text{DNet},k} \cos \psi_k \quad (8)$$

$$y_{k+1} = y_k + s_{\text{DNet},k} \sin \psi_k \quad (9)$$

where $s_{\text{DNet},k}$ denotes the distance estimated by D-Net at time step k , and ψ_k is the heading angle estimated by Madgwick filter.

It is worth mentioning that the MoRPINet does not provide velocity information.

III. PROPOSED MoRPI-PINN FRAMEWORK

In this work, we propose MoRPI-PINN, a novel pure inertial positioning framework designed for wheeled robots moving in periodic motion. MoRPI-PINN leverages the enforced maneuverability of such robots to learn the periodic trajectory patterns. A designed error-state observer, incorporating the 2D-INS equations of motion as physical constraints, is integrated into the model to enhance prediction accuracy. The MoRPI-PINN framework fuses these known physical constraints with sensor data to accurately track the trajectory of the mobile robot.

A. MoRPI-PINN Loss Function

The construction and optimization of the PINN loss function is critical for the success of the task at hand. In the training process of our MoRPI-PINN approach, the primary objective is to optimize the network parameters (weights and biases) to satisfy both the observed inertial sensor data and the underlying physical constraints enforced by the 2D-INS dynamics.

Our proposed neural network is parameterized by θ , which represents all trainable weights and biases of the network. During training, θ is optimized to minimize the total loss function, denoted as \mathcal{L} , integrates both a supervised loss ($\mathcal{L}_{\text{data}}$)

from accelerometers and gyroscopes measurements, and an unsupervised physics loss ($\mathcal{L}_{\text{phys}}$) derived from the 2D-INS equations of motion, along with initial condition loss ($\mathcal{L}_{\text{init}}$). Each of the sub-loss terms is described in detail below.

- **Data Loss:** Penalizes the discrepancy between the predicted states (position and velocity) and their GT counterparts. The data loss is calculated as the mean squared error (MSE) between the network's predictions and the GT values of the mobile robot 2D position and velocity vectors.

$$\mathcal{L}_{\text{data}} = \frac{1}{N_{\text{data}}} \sum_{i=1}^{N_{\text{data}}} \left(\|\mathbf{p}_i - \hat{\mathbf{p}}_i\|^2 + \|\mathbf{v}_i - \hat{\mathbf{v}}_i\|^2 \right), \quad (10)$$

where \mathbf{p}_i and \mathbf{v}_i represent the GT values of 2D position and velocity vectors of the mobile robot at data point i , respectively, while $\hat{\mathbf{p}}_i$ and $\hat{\mathbf{v}}_i$ denote the corresponding predicted vectors obtained from the network. The term N_{data} refers to the number of supervised training samples for which GT measurements are available.

- **Initial Condition Loss:** In order to ensure accurate trajectory estimation at the beginning of each input window, an initial condition loss is introduced. It penalizes discrepancies between the predicted initial position and its known initial values. It is computed as follows:

$$\mathcal{L}_{\text{init}} = \frac{1}{N_{\text{ic}}} \sum_{i=1}^{N_{\text{ic}}} \left(\|\hat{\mathbf{p}}_i - \mathbf{p}_0\|^2 \right), \quad (11)$$

where \mathbf{p}_0 is the initial position vector and N_{ic} is the number of samples used for enforcing the initial condition loss. Here, we set $N_{\text{ic}} = 200$, corresponding to 200 initial condition points used during training. These points are generated by repeating the first observed sensor readings from the training data.

- **Physics Loss:** In addition to the supervised learning losses, a physics-informed loss is incorporated into the model to ensure that the predictions of network are consistent with the underlying 2D-INS dynamics. The physics-informed residual loss function is calculated as:

$$\begin{aligned} \mathcal{L}_{\text{phys}} = \frac{1}{N_{\text{phys}}} \sum_{i=1}^{N_{\text{phys}}} & \left(\left\| \frac{d\hat{\mathbf{p}}^n(t_i; \theta)}{dt} - \hat{\mathbf{v}}^n(t_i; \theta) \right\|^2 \right. \\ & + \left\| \frac{d\hat{\mathbf{v}}^n(t_i; \theta)}{dt} - \left(\hat{\mathbf{C}}_b^n(t_i; \theta) \mathbf{f}_{ib}^b(t_i) + \mathbf{g}^n(t_i) \right) \right\|^2 \\ & \left. + \left\| \frac{d\hat{\mathbf{C}}_b^n(t_i; \theta)}{dt} - \hat{\mathbf{C}}_b^n(t_i; \theta) \mathbf{\Omega}_{ib}^b(t_i) \right\|_F^2 \right), \quad (12) \end{aligned}$$

where N_{phys} is number of collocation points used to enforce the underlying physical laws through the physics loss. Here, we generate a set of $N_{\text{phys}} = 2000$ collocation points, which are sampled uniformly across the time domain and randomly within the input sensor space. It ensures that the physics loss is evaluated not only at observed data points but also throughout the broader spatiotemporal domain; for generalization and consistency with the 2D-INS dynamics. Moreover, θ represents the set of trainable parameters of the neural network, and the notation $\|\cdot\|_F$ represents the Frobenius norm for matrices. This loss computes the

discrepancy between the network predicted dynamics and the true time derivative of the states, based on the physical model given in (1)–(3).

The physics loss can be expressed in explicitly as:

$$\begin{aligned} \mathcal{L}_{\text{phys}} = & \frac{1}{N_{\text{phys}}} \sum_{i=1}^{N_{\text{phys}}} \left[\left\| \frac{d}{dt} \begin{bmatrix} \hat{x}(t_i) \\ \hat{y}(t_i) \end{bmatrix} - \begin{bmatrix} \hat{v}_x(t_i) \\ \hat{v}_y(t_i) \end{bmatrix} \right\|^2 \right. \\ & + \left\| \frac{d}{dt} \begin{bmatrix} \hat{v}_x(t_i) \\ \hat{v}_y(t_i) \end{bmatrix} - \left(\mathbf{C}_b^n(\hat{\psi}(t_i)) \begin{bmatrix} f_x(t_i) \\ f_y(t_i) \end{bmatrix} + \begin{bmatrix} g_x \\ g_y \end{bmatrix} \right) \right\|^2 \\ & \left. + \left(\frac{d\hat{\psi}(t_i)}{dt} - \omega_z(t_i) \right)^2 \right], \end{aligned} \quad (13)$$

where $\hat{x}(t_i)$ and $\hat{y}(t_i)$ are predicted position components, respectively, $\hat{v}_x(t_i)$ and $\hat{v}_y(t_i)$ are predicted velocity components, respectively, and $\hat{\psi}(t_i)$ is predicted yaw angle. The 2D body to navigation rotation matrix $\mathbf{C}_b^n(\hat{\psi})$ is expressed as:

$$\mathbf{C}_b^n(\hat{\psi}) = \begin{bmatrix} \cos \hat{\psi} & -\sin \hat{\psi} \\ \sin \hat{\psi} & \cos \hat{\psi} \end{bmatrix}.$$

The total loss of our MoRPI-PINN model is a weighted sum of the above three components (10), (11), and (13):

$$\mathcal{L}_{\text{total}} = \lambda_{\text{data}} \mathcal{L}_{\text{data}} + \lambda_{\text{init}} \mathcal{L}_{\text{init}} + \lambda_{\text{phys}} \mathcal{L}_{\text{phys}}, \quad (14)$$

where λ_{data} , λ_{init} , and λ_{phys} are hyperparameters controlling the relative importance of each loss component. These weights are tuned to ensure that both empirical measurements and physical laws are adequately represented during training of neural network.

B. Network Architecture

The architecture of the MoRPI-PINN model for state estimation of mobile robots is designed to capture the intricate dynamics of navigation. To handle the sensors data and approximate a system of governing equations, dedicated DNN is designed. Its architecture consists of 10 hidden layers with 128 neurons each. We apply layer normalization on each layer and use the *SinTanh* nonlinear activation function [31]. The activation function $\phi(\cdot)$ is defined as:

$$\phi(z_i^{(\ell)}) = \sin(z_i^{(\ell)}) \cdot \tanh(z_i^{(\ell)}), \quad (15)$$

where z is the output layer defined by:

$$z_i^{(\ell)} = \sum_{j=1}^{n_{\ell-1}} \omega_{ij}^{(\ell)} a_j^{(\ell-1)} + b_i^{(\ell)}, \quad (16)$$

where $\theta = \{\omega^{[\ell]}, \mathbf{b}^{[\ell]}\}$, denotes the set of trainable parameters, ℓ is the index of the current layer, L is the total number of layers in the neural network, and n_ℓ represents the number of neurons in the ℓ^{th} layer.

Figure 1 illustrates the architecture of our proposed MoRPI-PINN framework for mobile robot pure inertial navigation. The network receives time (t), specific force measurements from the accelerometer (f_x , f_y), and angular velocity from the gyroscope (ω_z) as inputs. These are processed through a fully connected neural network to predict the robot's 2D position (\hat{x} , \hat{y}), velocity (\hat{v}_x , \hat{v}_y), and yaw angle ($\hat{\psi}$), collectively denoted as $\hat{\mathbf{N}}$.

C. Training Process

Since the PINNs approach is mesh-free, the scattered training points have been employed instead of lattice-like structured points. This provides the network more flexibility for training of complex trajectories. The model has been trained for 1,000 epochs using a batch size of 32 and an initial learning rate of 0.001. To enhance generalization and prevent overfitting, dropout was applied with a rate of 0.2. A learning rate scheduler reduced the learning rate (η) by a factor of 0.5 if the validation loss plateaued for 50 epochs, enabling broad initial adjustments. Early stopping was implemented with a patience to prevent overfitting. The inertial data were segmented using overlapping windows of 10 samples with an overlap of 12 samples between successive segments to preserve temporal coherence.

TABLE I
MORPI-PINN HYPERPARAMETERS

Hyperparameter	Value
Learning Rate	0.001
Batch Size	32
Epochs	1000
Hidden Layers	10
Neurons per Layer	128
Dropout Rate	0.2

During the training, network parameters θ are optimized using the Adam optimizer, known for its efficacy in handling complex optimization challenges. The optimizer has employed with weight decay ($1e - 04$) to provide $L2$ regularization. The estimated state ($\hat{\mathbf{N}}(t)$) and its derivative with respect to the trainable parameters are derived through the PINNs framework. The hyperparameters used for training the MoRPI-PINN model are summarized in Table I. The configuration of our hardware used for training the models is summarized in Table II. The MoRPI-PINN training process is summarized in Algorithm 1.

TABLE II
HARDWARE SETUP: GPU SPECIFICATIONS FOR MODEL TRAINING

Parameter	Details
GPU Model	NVIDIA GeForce RTX 4090
CUDA Version	12.6
Driver Version	560.35.05
Memory Size	24 GB
Tensor Cores	512
Compute Capability	8.9
Operating System	macOS 15.4.1

IV. ANALYSIS AND RESULTS

We begin by describing the dataset used in our analysis followed by a definition of evaluation matrices. Then, we conduct a thorough analysis of our proposed approach and compare it to the model-based baseline (2D-INS) and the data-driven baseline (MoRPI-Net).

A. Dataset

The experimental GT data were collected from a field experiment conducted by Etzion et al. [20]. In this experiment, a RC car, model STORM Electric 4WD Climbing Car, was employed (Figure 2). The car has dimensions of $385 \times 260 \times 205$ mm, a

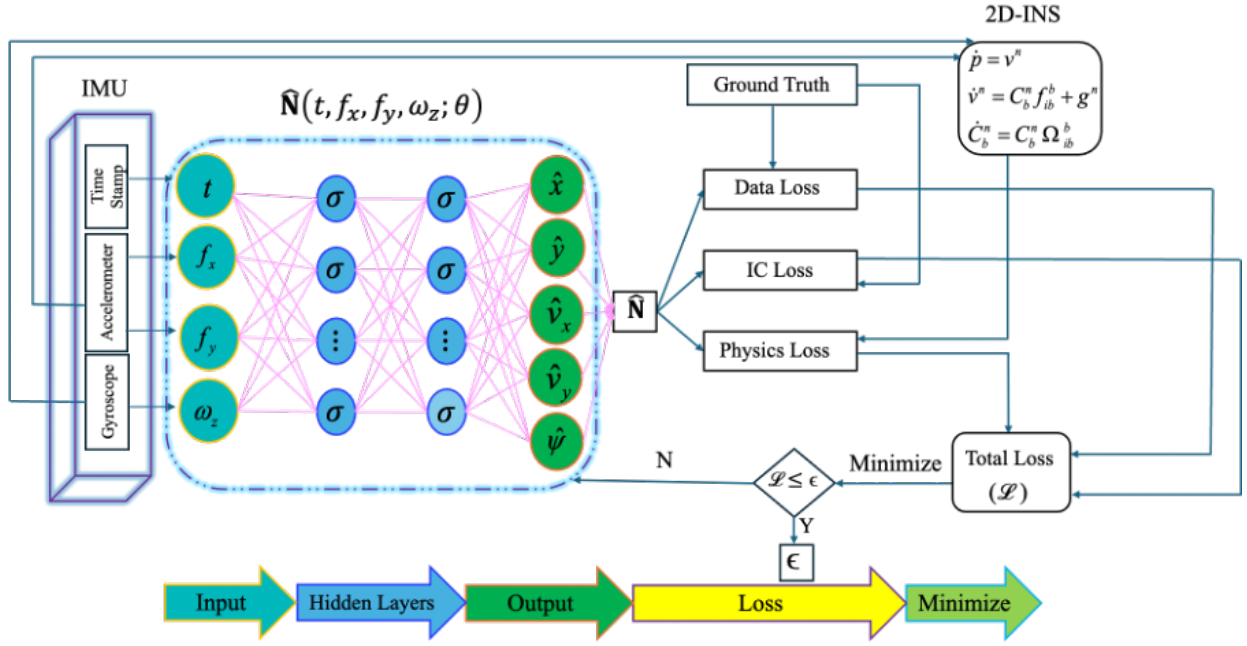


Fig. 1. Illustration of the proposed MoRPI-PINN framework training process.

Algorithm 1 MoRPI-PINN training process

- 1: **Input:** Initial weights \mathbf{w}_0 , biases \mathbf{b}_0
- 2: **Given:**
 - Supervised data $\{t_i, \mathbf{x}_{\text{true}}(t_i)\}_{i=1}^{N_{\text{data}}}$
 - Initial state \mathbf{x}_0 at $t = 0$
 - Collocation points $\{t_j\}_{j=1}^{N_{\text{phys}}}$
- 3: **Initialize:** Iteration counter $k \leftarrow 0$, convergence threshold ϵ
- 4: **while** not converged **do**
- 5: Predict: $\hat{\mathbf{x}}(t)$ using current network parameters
- 6: Compute total loss: $\mathcal{L}_{\text{total}}$ according to (14)
- 7: Update network parameters using suitable optimizer
- 8: **if** change in $\mathcal{L}_{\text{total}} < \epsilon$ **then**
- 9: **break**
- 10: **end if**
- 11: $k \leftarrow k + 1$
- 12: **end while**



Fig. 2. RC car used in the experiments mounted with RTK GNSS and IMUs.

wheelbase of 253 mm, and a tire diameter of 110 mm. The RC car was equipped with a *Javad SIGMA-3N* RTK GNSS sensor [32], providing high-accuracy positioning measurements with an accuracy of 10 cm at a sample rate of 10 Hz, serving as the GT. Additionally, the RC car was mounted with *Movella DOT* IMUs, capable of operating at 120 Hz [33]. Further details regarding the dataset are provided in [20]. Since the IMU operates at a frequency of 120 Hz and the RTK at 10 Hz, one RTK sample corresponds to twelve IMU samples. The associated noise and bias values of the accelerometer and gyroscope are presented in Table III.

The training trajectory, shown in Figure 3, spans a duration of 794 sec and serves as the primary data for the training. The testing dataset comprises four trajectories from the same

TABLE III
MOVELLA DOT IMU SPECIFICATIONS [33].

Specification	Gyroscope	Accelerometer
Bias	10 $^{\circ}$ /h	0.03 mg
Noise Density	0.007 $^{\circ}$ /s/ $\sqrt{\text{Hz}}$	120 $\mu\text{g}/\sqrt{\text{Hz}}$

experimental study [20], collectively covering approximately 25 m. These trajectories include both straight-line and periodic motion patterns. The four test trajectories, depicted in Figure 4, were recorded over 37, 46, 39, and 70 sec, respectively, totaling 192 sec of inertial data. The same dataset is used for evaluating the baseline methods and our proposed MoRPI-PINN

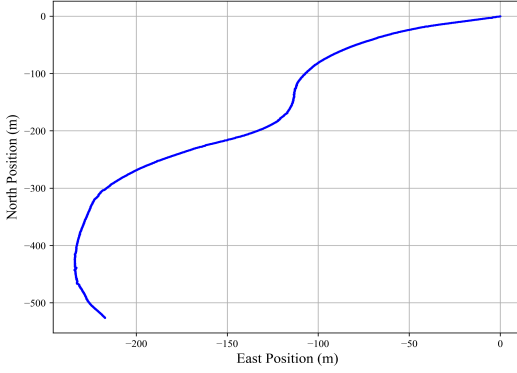


Fig. 3. The single ground-truth trajectory of the training set spans 794 sec.

framework.

A total of 200 initial condition points are incorporated into training. These are synthetically generated by duplicating the first observed sensor readings from the training trajectory (Figure 3) to provide stable initialization across collocation samples. Moreover, prior to training and testing, the data underwent the following preprocessing pipeline:

- 1) The first 60 sec of data were removed for initial stabilization.
- 2) A new time stamp starting from 0 sec was assigned according to the sampling frequency of the corresponding sensors.
- 3) Each axis was normalized independently using its respective direction.

B. Evaluation Metrics

For our analysis, we use the following evaluation metrics:

- **Absolute Trajectory Error (ATE):**

$$\text{ATE}(\mathbf{p}_i, \hat{\mathbf{p}}_i) = \sqrt{\frac{1}{N} \sum_{i=1}^N (\mathbf{p}_i - \hat{\mathbf{p}}_i)^2}, \quad (17)$$

where \mathbf{p}_i and $\hat{\mathbf{p}}_i$ are the GT position vector, and the predicted position vector, respectively, i is the time index, and N is the total number samples.

- **Velocity Root Mean Squared Error (VRMSE):**

$$\text{VRMSE}(\mathbf{v}_i, \hat{\mathbf{v}}_i) = \sqrt{\frac{1}{N} \sum_{i=1}^N (\mathbf{v}_i - \hat{\mathbf{v}}_i)^2}. \quad (18)$$

where \mathbf{v}_i and $\hat{\mathbf{v}}_i$ are the GT velocity vector, and the predicted velocity vector, respectively, i is the time index, and N is the total number samples.

- **Normalized Velocity Root Mean Squared Error (NVRMSE):**

$$\text{NVRMSE} = \frac{\text{VRMSE}}{\|\mathbf{v}_{\max}\| - \|\mathbf{v}_{\min}\|}, \quad (19)$$

where \mathbf{v}_{\max} and \mathbf{v}_{\min} represent the maximum and minimum values of the GT velocity vector across the entire training dataset. NVRMSE scales VRMSE by the range of the GT data, enabling cross dataset comparisons and unit-free error interpretation.

C. Performance Analysis

Before diving into the results, we note that for mobile robot positioning performance we compare our approach to both baseline methods. However, for velocity comparison, only the 2D-INS model is considered, as MoRPINet does not provide velocity information. The 2D-INS does using (1)–(3), while MoRPINet was evaluated under the same conditions for comparative analysis. To improve baseline accuracy, zero-order calibration was applied to the accelerometer and gyroscope data by leveraging the initial stationary segment of each trajectory. In contrast, the proposed MoRPI-PINN model and MoRPINet used raw sensor data, in order to demonstrate the capability to operate effectively in noisy conditions.

All three approaches were evaluated on the test dataset which consist of four different trajectories: straight-line trajectory (Figure 4a), periodic trajectories (Figures 4b–4c), and the L-shaped path (Figure 4d).

1) *2D-INS*: The 2D-INS solution was evaluated, as it is one of the most widely adopted baseline models in navigation systems. As anticipated, it produced significant errors. For position estimation, the model yields an average ATE of 14.3 m across the test dataset.

Furthermore, the accuracy of 2D-INS model in velocity estimation is notably poor, with NVRMSE reaching 1077% for v_x and 1211% for v_y in the straight-line trajectory. In the periodic trajectories, the errors remain high, with 51% and 1060% for v_x , and 37% and 2149% for v_y , in Trajectories 2 and 3, respectively. The challenges posed by the L-shaped trajectory further amplify these errors, with NVRMSEs reaching 277% for v_x and 175% for v_y . These results highlight the limitations of the model-based dead-reckoning approach, in handling long durations under dynamic motion, and sharp turns.

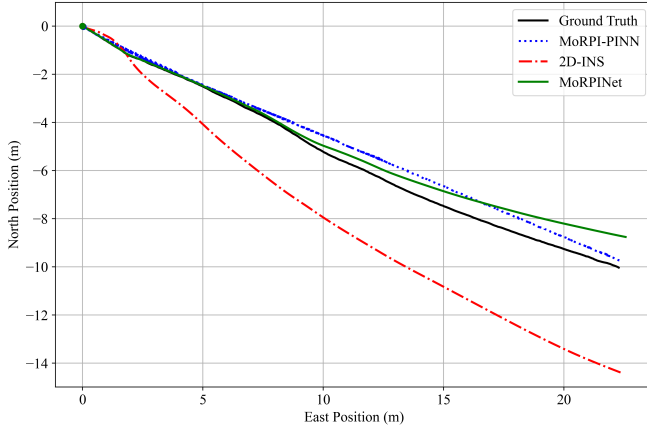
2) *MoRPINet*: The data-driven MoRPINet serves as a strong baseline method for navigation, offering a significant improvement in position estimation accuracy over traditional 2D-INS. The data-driven MoRPINet achieves accuracy of 85%, with an average ATE of 5.7 m across all trajectories. This demonstrates the potential of deep learning models to correct inertial drift by capturing data patterns directly from sensor inputs.

Moreover, despite its gains in position estimation, it still struggles in scenarios involving sudden directional changes, where its predictions deviate more significantly.

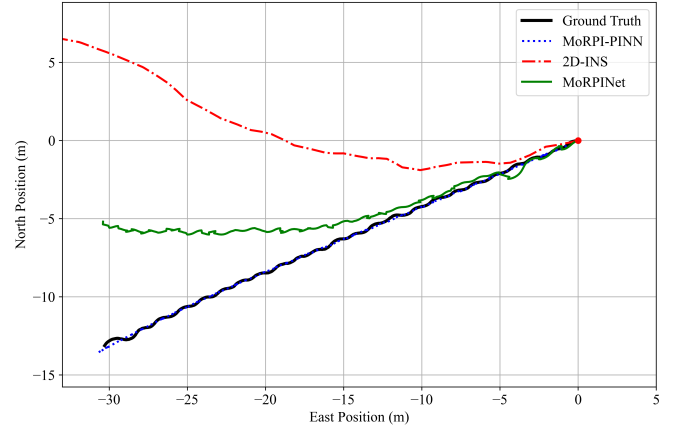
3) *MoRPI-PINN*: Achieves comparatively low ATEs across all trajectories, with an average ATE of 0.8 m, resulting in 94% improvement over 2D-INS and 85% improvement over MoRPINet.

In terms of velocity estimation, MoRPI-PINN demonstrates consistently low NVRMSEs. For the straight-line trajectory, it achieves 54% in v_x and 25% in v_y . In the periodic motion trajectories, NVRMSEs are 34% (v_x) and 49% (v_y) for Trajectory 2, and 37% (v_x) and 35% (v_y) for Trajectory 3. For the L-shaped trajectory, the model further reduces the errors to 20% in v_x and 24% in v_y .

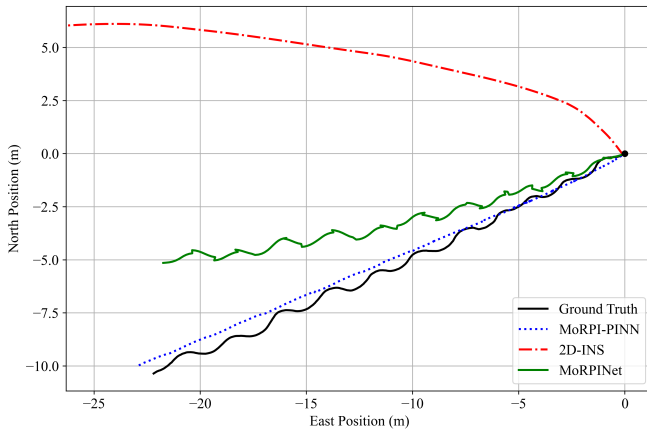
These results highlight the robustness and generalizability of MoRPI-PINN across a diverse set of trajectories. It demonstrates the advantages of integrating physics of 2D-INS equations of motion for accurate mobile robot navigation under challenging



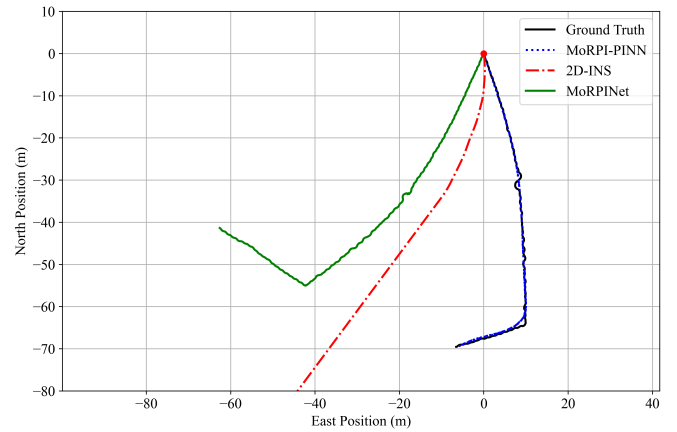
(a) Trajectory 1



(b) Trajectory 2



(c) Trajectory 3



(d) Trajectory 4

Fig. 4. Ground truth trajectory of the test dataset with the estimated trajectory from the model-based baseline (2D-INS), data-driven baseline (MoRPINet), and our MoRPI-PINN method.

dynamics.

D. Summary

Across all evaluated scenarios, MoRPI-PINN framework consistently and significantly outperforms the baseline models. As shown in Table IV, MoRPI-PINN framework improved the ATE of the 2D-INS by 94% and MoRPINet by 85%. The model also demonstrates excellent dead-reckoning accuracy, with a maximum ATE of 1.1 m, across all testing trajectory as shown in Figure 5. The maximum errors remain low due to the constraints imposed by physics-informed learning in the term of the physics loss ($\mathcal{L}_{\text{phys}}$) from 2D-INS equation. In contrast to traditional 2D-INS algorithms, where errors accumulate over time, MoRPI-PINN exhibits only occasional larger deviations. So model effectively mitigates long-term drift, a critical limitation in traditional inertial navigation approach.

Furthermore, low initial condition loss ($\mathcal{L}_{\text{init}} \approx 10^{-3}$) ensures accurate trajectory initialization ($x(0), y(0) \approx 0$), helping to reduce ATE at the beginning of the trajectory. Input normalization enables consistent performance across a range of accelerometer (f_x, f_y) and gyroscope (ω_z) data and reducing errors in diverse test scenarios. Here, the physics-informed loss ($\mathcal{L}_{\text{phys}}$), again

plays a key role for capturing the underlying dynamics. This regularization helps prevent overfitting to noisy measurements; a common limitation of purely data-driven neural networks.

These results emphasize the potential of physics-informed learning to significantly enhance inertial navigation, especially in scenarios where sensor calibration is impractical or where the motion deviates from simple linear dynamics.

V. CONCLUSION

In real-world scenarios, GNSS-denied environments and poor lighting conditions result in pure inertial navigation and thus rapid drift in position solution. To mitigate this drift, we introduced the MoRPI-PINN framework. Our approach integrates 2D-INS governing equations into the neural network training process. It employs compound loss combining data loss, physical loss, and initial condition loss. This design enables robust learning even in the presence of sensor error terms and noise.

We assessed MoRPI-PINN across four real-world trajectories and compared it against two existing model-based methods: (1) a traditional numerical 2D-INS solution, and (2) the data-driven MoRPINet approach. MoRPI-PINN achieved a position error of just 0.8 m, significantly outperforming 2D-INS (14.3 m)

TABLE IV
ABSOLUTE TRAJECTORY ERROR(M) OVER FOUR TRAJECTORIES WITH AVERAGE AND IMPROVEMENT

Approach	ATE [m]				Average	Improvement
	Trajectory 1	Trajectory 2	Trajectory 3	Trajectory 4		
2D-INS (model-based baseline)	11.2	7.1	11.3	27.9	14.3	94%
MoRPINet (data-driven baseline)	5.8	5.1	5.4	6.6	5.7	85%
MoRPI-PINN (ours)	1.1	0.9	0.9	0.4	0.8	–

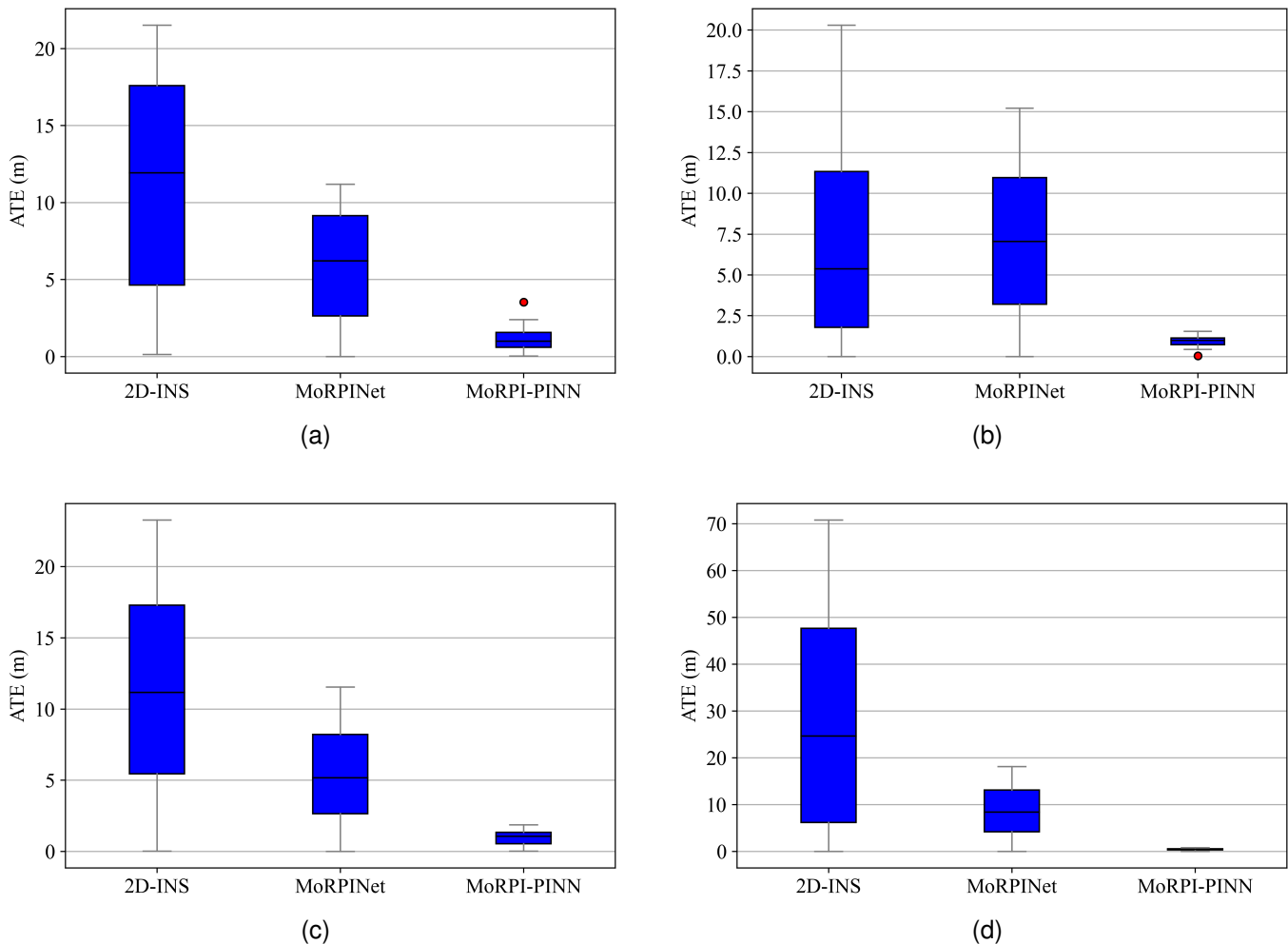


Fig. 5. ATE across the four test trajectories for the model-based baseline (2D-INS), data-driven baseline (MoRPINet), and our MoRPI-PINN method.

and MoRPINet (5.7 m). This corresponds to 94% improvement over the 2D-INS solution and 85% improvement over the MoRPINet baseline. Moreover, MoRPI-PINN demonstrated robust performance in unstructured and low-calibration environments, where conventional methods typically experience drift and bias accumulation. These results demonstrate that MoRPI-PINN is a robust solution for mobile robot state estimation in GNSS denied conditions. Its ability to simultaneously leverage physical constraints and data-driven learning allows it to overcome the limitations of both purely analytical and purely data-based methods. A potential limitation is that MoRPI-PINN may exhibit slightly higher ATE in data-rich scenarios, as strict adherence to physics may reduce adaptability to rapid pattern changes in

the data.

Overall, the proposed model is well-suited to a wide range of real-world mobile robot applications, including manufacturing and logistics, security and surveillance, delivery services and infrastructure inspection. MoRPI-PINN is lightweight, yet has an effective architecture making it ideal for deployment on embedded platforms, enabling real-time navigation in adversarial environments. Thus, MoRPI-PINN effectively bridges the limitations of pure inertial navigation, and enables seamless robot navigation using inertial sensor data during short time-periods.

ACKNOWLEDGEMENT

A. K. S. was supported by the Maurice Hatter Foundation.

REFERENCES

- [1] X. Gao, J. Li, L. Fan, Q. Zhou, K. Yin, J. Wang, C. Song, L. Huang, and Z. Wang, "Review of wheeled mobile robots' navigation problems and application prospects in agriculture," *IEEE Access*, vol. 6, pp. 49 248–49 268, 2018.
- [2] N. Shalal, T. Low, C. McCarthy, and N. Hancock, "A review of autonomous navigation systems in agricultural environments," *SEAG 2013: Innovative Agricultural Technologies for a Sustainable Future*, 2013.
- [3] D. Hurwitz, N. Cohen, and I. Klein, "Deep learning assisted inertial dead reckoning and fusion," *IEEE Transactions on Instrumentation and Measurement*, 2024.
- [4] P. Rao, D. Mohapatra, S. Chakraverty, and D. Roy, "Vibration analysis of non-homogenous single-link flexible manipulator in uncertain environment," *Applied Mathematical Modelling*, vol. 141, p. 115939, 2025.
- [5] G. N. DeSouza and A. C. Kak, "Vision for mobile robot navigation: A survey," *IEEE Transactions on Pattern Analysis and Machine Intelligence*, vol. 24, no. 2, pp. 237–267, 2002.
- [6] Y. Cheng and G. Y. Wang, "Mobile robot navigation based on lidar," in *2018 Chinese control and decision conference (CCDC)*. IEEE, 2018, pp. 1243–1246.
- [7] A. Tsalatsanis, K. Valavanis, and N. Tsourveloudis, "Mobile robot navigation using sonar and range measurements from uncalibrated cameras," *Journal of Intelligent and Robotic Systems*, vol. 48, pp. 253–284, 2007.
- [8] T. Suzuki, M. Kitamura, Y. Amano, and N. Kubo, "Autonomous navigation of a mobile robot based on GNSS/DR integration in outdoor environments," *Journal of Robotics and Mechatronics*, vol. 26, no. 2, pp. 214–224, 2014.
- [9] H. Maaref and C. Barret, "Sensor-based navigation of a mobile robot in an indoor environment," *Robotics and Autonomous Systems*, vol. 38, no. 1, pp. 1–18, 2002.
- [10] D. Nemeč, M. Hrubos, A. Janota, R. Pirnik, and M. Gregor, "Estimation of the speed from the odometer readings using optimized curve-fitting filter," *IEEE Sensors Journal*, vol. 21, no. 14, pp. 15 687–15 695, 2020.
- [11] D. Titterton and J. L. Weston, *Strapdown inertial navigation technology*. IET, 2004, vol. 17.
- [12] J. L. Farrell, *GNSS aided navigation & tracking: inertially augmented or autonomous*. American Literary Press Baltimore, Maryland, 2007.
- [13] A. Shurin and I. Klein, "QDR: A quadrotor dead reckoning framework," *IEEE Access*, vol. 8, pp. 204 433–204 440, 2020.
- [14] I. Klein, "Pedestrian inertial navigation: An overview of model and data-driven approaches," *Results in Engineering*, p. 104077, 2025.
- [15] X. Liu, Y. Zhang, N. Li, Y. Huang, and Y. Zhao, "A novel pedestrian dead-reckoning algorithm with self-estimates of imu biases," *IEEE Transactions on Instrumentation and Measurement*, 2025.
- [16] A. Etzion and I. Klein, "MoRPI: Mobile robot pure inertial navigation," *IEEE Journal of Indoor and Seamless Positioning and Navigation*, vol. 1, pp. 141–150, 2023.
- [17] N. Cohen and I. Klein, "Inertial navigation meets deep learning: A survey of current trends and future directions," *Results in Engineering*, p. 103565, 2024.
- [18] C. Chen and X. Pan, "Deep learning for inertial positioning: A survey," *IEEE Transactions on Intelligent Transportation Systems*, vol. 25, no. 9, pp. 10 506–10 523, 2024.
- [19] A. Shurin and I. Klein, "QuadNet: A hybrid framework for quadrotor dead reckoning," *Sensors*, vol. 22, no. 4, p. 1426, 2022.
- [20] A. Etzion, N. Cohen, O. Levi, Z. Yampolsky, and I. Klein, "Snake-inspired mobile robot positioning with hybrid learning," *Scientific Reports*, vol. 15, no. 1, p. 15602, 2025.
- [21] M. Raissi, P. Perdikaris, and G. E. Karniadakis, "Physics-informed neural networks: A deep learning framework for solving forward and inverse problems involving nonlinear partial differential equations," *Journal of Computational Physics*, vol. 378, pp. 686–707, 2019.
- [22] D. Dwivedi, P. K. Yemula, and M. Pal, "Dynamopmu: A physics informed anomaly detection, clustering, and prediction method using nonlinear dynamics on μ pmu measurements," *IEEE Transactions on Instrumentation and Measurement*, vol. 72, pp. 1–9, 2023.
- [23] W. H. Lim, S. Sfarra, T.-Y. Hsiao, and Y. Yao, "Physics-informed neural networks for defect detection and thermal diffusivity evaluation in carbon fiber reinforced polymer using pulsed thermography," *IEEE Transactions on Instrumentation and Measurement*, 2025.
- [24] S. Kumar, A. K. Sahoo, and S. Chakraverty, "Physics-informed machine learning framework for approximating the modified degasperis-procesi equation," in *2023 International Conference on Ambient Intelligence, Knowledge Informatics and Industrial Electronics (AIKIE)*. IEEE, 2023, pp. 1–6.
- [25] A. K. Sahoo, S. Kumar, and S. Chakraverty, "An unsupervised scientific machine learning algorithm for approximating displacement of object in mass-spring-damper systems," *IEEE Access*, 2024.
- [26] Y. Guo, H. Zou, F. Wei, Q. Li, D. Guo, and J. Pirov, "Analysis of pedestrian second crossing behavior based on physics-informed neural networks," *Scientific Reports*, vol. 14, no. 1, p. 21278, 2024.
- [27] W. Gu, S. Primatesta, and A. Rizzo, "Physics-informed neural network for quadrotor dynamical modeling," *Robotics and Autonomous Systems*, vol. 171, p. 104569, 2024.
- [28] S. Park and S. Lee, "State observer-based physics-informed machine learning for leader-following tracking control of mobile robot," *ISA Transactions*, vol. 146, pp. 582–591, 2024.
- [29] P.-F. Xu, C.-B. Han, H.-X. Cheng, C. Cheng, and T. Ge, "A physics-informed neural network for the prediction of unmanned surface vehicle dynamics," *Journal of Marine Science and Engineering*, vol. 10, no. 2, p. 148, 2022.
- [30] P. Groves, "Book principles of GNSS, inertial and multi-sensor integrated navigation systems, 2nd (ed) artech house: London," 2013.
- [31] A. K. Sahoo and S. Chakraverty, "Machine intelligence in dynamical systems: A state-of-art review," *Wiley Interdisciplinary Reviews: Data Mining and Knowledge Discovery*, p. e1461, 2022.
- [32] Javad, "Javad SIGMA-3N," <https://www.javad.com/jgnss/products/receivers/sigma.html>, accessed: 2022-10-01.
- [33] Xsens, "Xsens DOT," <https://www.xsens.com/xsens-dot>, accessed: 2022-10-01.